Digital Homing Guidance—Stability vs Performance Tradeoffs

F. William Nesline Jr.* and Paul Zarchan†
Raytheon Company, Bedford, Massachusetts

Digital signal processing capability can be added to a missile homing guidance system to provide a broad system decision capability against a complex threat. This processing may be on the ground or in the missile. Wherever it occurs, it introduces additional dynamics into the guidance loop which can degrade system performance. In fact, the influence of digitization is so important that it must be included at the outset in order to ensure that a guidance system design will work. One of the most significant effects is the introduction of a sample and hold in the guidance attitude loop. This paper discusses the influence of digital processing on system relative stability and performance. A variety of techniques for improving system performance are introduced and tradeoff curves are presented indicating how major subsystem parameters, such as seeker stabilization loop gain or autopilot time constant, may be specified. The results show the tradeoffs between a robust set of guidance subsystem specifications and acceptable performance when digital guidance is used.

Introduction

WHEN homing guidance systems are built, component imperfections create unwanted parasitic paths that can lead to guidance instability.[1] Analog homing systems are designed by the specification of proper values and tolerances on such critical parameters in the parasitic loops as radome refraction slope, seeker gyro acceleration sensitivity, seeker stabilization loop gain, and missile aerodynamic turning time constant.[2,3] A proper set of values and tolerances guarantees stable performance over the range of engagement parameters and flight conditions needed to intercept the targets. When digital guidance is used, the main guidance loop must be broken in order to insert an A/D converter, a signal processor, and a D/A converter. These components change the response characteristics of the homing loop; therefore; tradeoff studies must be conducted at the outset in order to ensure that the guidance system will work.

To first order, the A/D converter, signal processor, and D/A converter can be approximated by a sample and hold network. This paper uses frequency response techniques to investigate the impact of this network on the relative stability of the homing loop and to suggest methods of compensation. Time domain adjoints[4] are then used to measure miss distance and to quantify the robustness properties of the homing loop.

Continuous Analysis

The planar dynamics of the radar homing system shown in Fig. 1 indicate the dynamics of the various parts of the missile guidance system. The seeker contains a tracking loop and a simplified stabilization loop. In addition, parameters that represent unwanted, or parasitic, feedback paths for radome refraction slope and for gyro acceleration sensitivity are shown. The processor is represented by a sampler and zero order hold and may be in the missile or on the ground if a suitable downlink and uplink are included. The noise filter attenuates the radar boresight error noise to develop a smoothed estimate of the line-of-sight rate estimate into acceleration commands for the flight control system.[5,6] The seeker has a gyro controlled stabilization loop to prevent missile pitching motion from contaminating the line-of-sight rate to the target. Figure 1 shows a first-order stabilization loop consisting of a gain and an integrator. The degree of stabilization achieved depends upon the gain K_{SL}. For such a stabilization loop, K_{SL} is also the stabilization bandwidth.

The concept of the open-loop transfer function is the cornerstone of feedback control system analysis. Nyquist[7] showed its importance in stability and robustness analysis, and Bode[8] developed its use as a key design and synthesis element in feedback systems. The open-loop transfer function is the transfer function around the loop when the loop is broken at a point. The loop can be broken anywhere, but is usually broken in series with some parameter whose value the designer can control to achieve a desired characteristic. While the whole open-loop transfer is interesting, its frequency response characteristic is most illuminating to the designer. Both relative stability and robustness can be determined from analysis of the magnitude and phase of the open-loop frequency response, and, even more important, the designer can determine from it what changes to make in the system dynamics in order to achieve his goals.

The two most popular indices of relative stability are the gain margin and the phase margin. The gain margin is the value of additional gain needed at the loop break to cause instability, assuming that the phase remains constant. The phase margin is the amount of phase lag that is needed at the loop break to cause instability, assuming that the gain remains constant. In multiloop systems it may be desirable or necessary to break the loop in many places and to analyze the loop frequency response in each place in order to ensure proper relative stability of the whole system. This is the case in this paper. The authors are interested in the effects of digitization

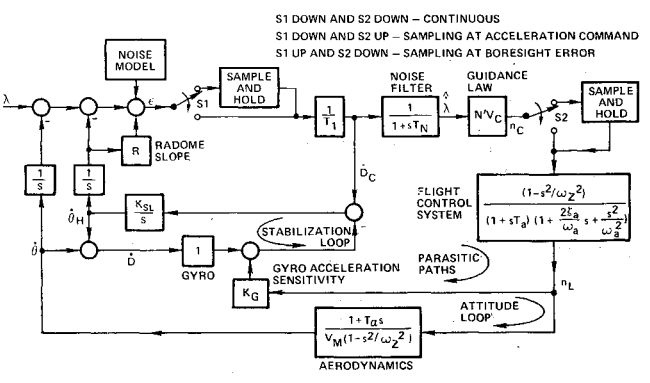

Fig. 1 Missile system dynamics.

Presented as Paper 83-2167 at the AIAA Guidance and Control Conference, Gatlinburg, Tenn., Aug. 15-17, 1983; received Aug. 24, 1983; revision received Jan. 4, 1984.

*Chief Systems Engineer, Missile Systems Division. Associate Fellow AIAA.

†Principal Engineer, Missile Systems Division. Member AIAA.

at two places in the system. The first is at the guidance command, which is a relatively low bandwidth point at which the designer can accept guidance measurements and convert them to guidance commands. The second point is at the seeker boresight error. This is a higher bandwidth point, which the designer may be required to accept because of the nature of the system.

With switches S1 and S2 down, the model is continuous. The attitude open-loop transfer function, with the loop broken at the acceleration command, neglecting radome refraction slope and gyro acceleration sensitivity, can be obtained from Fig. 1 and is approximated by the following transfer function:

$$HG(S)|_{\eta_c} \simeq N'V_c S(1+ST_\alpha) \div \left[K_{SL}V_M(1+ST_I)(1+S/K_{SL})(1+ST_N)(1+ST_a) \times \left(1+\frac{2\zeta_a}{\omega_a}S+\frac{S^2}{\omega_a^2}\right)\right] \quad (1)$$

where N' is the effective navigation ratio, V_c is the closing velocity, and T_I and T_N are the seeker and noise filter time constants. The nonminimum phase zero, ω_z in Fig. 1, is determined by the aerodynamic configuration and is typical of tail-controlled missiles. It does not enter into the loop transmission. The flight control system (autopilot) time constant, T_a, damping, ζ_a, and natural frequency, ω_a, are typical parameters in an operational three-loop autopilot.

For this system, the tracking time constant is set by seeker tracking dynamics, the noise filter time constant is set by radar signal and noise spectral content, the effective navigation ratio is set by knowledge of the properties of proportional navigation, the closing velocity is measured by the radar using Doppler or range rate information, the flight control zeroes are determined by the missile, and the three flight control poles are determined by the missile and the flight control system, i.e., the aerodynamics, the structural dynamics, the actuators, the instruments, and the autopilot gains. The frequency of the quadratic autopilot pole pair is determined by the aerodynamic moment slope with respect to angle of attack (M_α); the damping of the quadratic pair is set by stability considerations. Therefore, the autopilot real pole is the primary adjustable parameter for the ideal guidance system.

With the nominal inputs described in Table 1 and a nominal autopilot time constant of 0.6 s, the attitude open-loop transfer function becomes

$$HG(S)|_{nc} \simeq 0.06\{S(1+S/0.5) \div \left[(1+S/10)(1+S/100)(1+S/6.67)(1+S/1.67) \times \left(1+\frac{2*0.7}{20}S+\frac{S^2}{20^2}\right)\right]\} \quad (2)$$

Table 1 Nominal inputs

Symbol	Definition	Value
T_α	Aerodynamic turning rate time constant	2 s
T_I	Seeker tracking time constant	0.1 s
T_N	Noise filter time constant	0.15 s
N'	Effective navigation ratio	3
V_c	Closing velocity	5000 ft/s
V_M	Missile velocity	2500 ft/s
ω_z	Flight control system zero	30 rad/s
ω_a	Flight control system natural frequency	20 rad/s
ζ_a	Flight control system damping	0.7
K_{SL}	Stabilization loop gain	100 rad/s

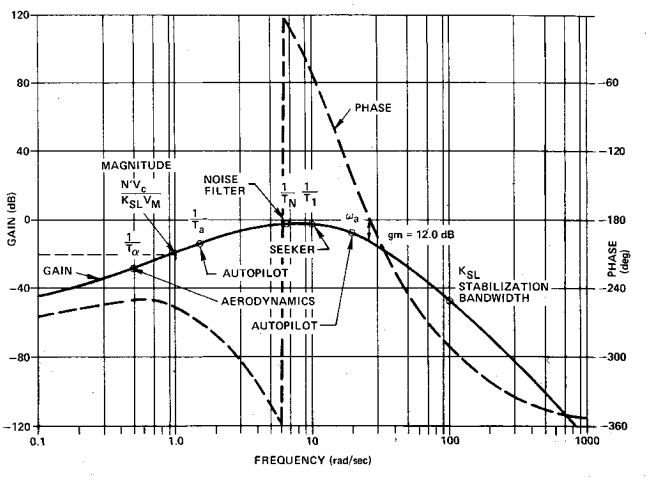

Fig. 2 Continuous frequency response for breaking loop at acceleration command (T_a = 0.6 s).

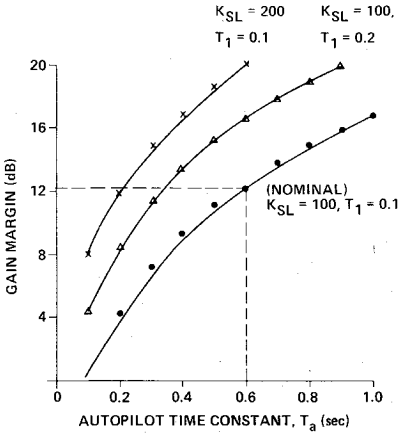

Fig. 3 Stability margins improve with increasing time constants and stabilization loop gain (loop broken at acceleration command).

Figure 2 shows a frequency response of an attitude loop broken at the acceleration command with significant frequencies of all the components marked. Since the gain is always below 0 dB, the phase margin is infinite. In other words, with the autopilot gain held constant, no amount of phase lag added to the loop will cause the closed-loop response to go unstable. For the parameters used, the gain margin is 12 dB. This gain margin degrades as the autopilot time constant (or any of the other time constants) is reduced. In addition, the gain constant of this attitude loop is $(N'V_c/K_{SL}V_M)$. Therefore the gain margin improves as the stabilization loop gain increases. The influence of time constants and stabilization loop gain on loop relative stability is displayed in Fig. 3. Increasing stabilization loop gain, seeker time constant, or autopilot time constant improves the gain margin. Of course, there is a cost penalty associated with increasing the stabilization loop gain. Increasing the seeker time constant can result in loss of track against severely maneuvering targets, while increasing the autopilot time constant results in increased miss distance against maneuvering targets. Figure 3 shows that for a stabilization loop gain of 100 the autopilot time constant required to yield a 12 dB gain margin (to leave room for sampling degradation) is 0.6 s. Doubling the loop gain reduces this autopilot time constant requirement to 0.2 s. This means that with a stabilization loop gain of 100 and autopilot time constant of 0.6 s, the autopilot gain could be increased by a factor of 4 (12 dB) before the closed-loop response goes unstable. With a stabilization loop gain of 200 and an autopilot time constant of 0.2 s, the autopilot gain could also be

increased by a factor of 4 (12 dB) before the closed-loop response goes unstable.

If the attitude loop is broken at the boresight error ϵ, the open-loop transfer function can be obtained from Fig. 1 as

$$HG(S)|_\epsilon = \frac{1}{T_I}\left\{(1+ST_N)(1+ST_a)\left(1+\frac{2\zeta_a}{\omega_a}S+\frac{S^2}{\omega_{a^2}}\right)\right.$$
$$+\frac{N'V_c}{V_M K_{SL}}S(1+T_aS)\Big/\left[S(1+SK_{SL})\right.$$
$$\left.\left.\times(1+ST_N)(1+ST_a)\left(1+\frac{2\zeta_a}{\omega_a}S+\frac{S^2}{\omega_{a^2}}\right)\right]\right\} \quad (3)$$

Expansion of the transfer function numerator yields

$$HG(S)|_\epsilon = \frac{1}{T_I}\left\{\left[1+S\left(T_N+T_a+\frac{2\zeta_a}{\omega_a}+\frac{N'V_c}{V_M K_{SL}}\right)\right.\right.$$
$$+S^2\left[T_aT_N+\frac{2\zeta_a}{\omega_a}(T_N+T_a)+\frac{1}{\omega_{a^2}}+\frac{N'V_cT_a}{V_M K_{SL}}\right]$$
$$+S^3\left[\frac{2\zeta_a}{\omega_a}T_aT_N+\frac{1}{\omega_{a^2}}(T_N+T_a)\right]+S^4\frac{T_aT_N}{\omega_{a^2}}\Big]$$
$$\left.\div\left[S(1+S/K_{SL})(1+T_N)(1+ST_a)\left(1+\frac{2\zeta_a}{\omega_a}S+\frac{S^2}{\omega_{a^2}}\right)\right]\right\} \quad (4)$$

With the nominal inputs of Table 1 and an autopilot time constant of 0.6 s, the open-loop transfer function becomes

$$HG|_\epsilon = 10\left\{1+0.88S+0.265S^2+0.008175S^3+0.000225S^4\right.$$
$$\div\left[S(1+S/100)(1+S/6.67)(1+S/1.67)\right.$$
$$\left.\left.\times\left(1+\frac{2*0.7}{20}S+\frac{S^2}{20^2}\right)\right]\right\} \quad (5)$$

Finding the roots of the numerator yields

$$HG|_\epsilon = 10\left\{\left(1+\frac{2*0.87}{2.05}S+\frac{S^2}{2.05^2}\right)\left(1+\frac{2*0.5}{32.5}S+\frac{S^2}{32.5^2}\right)\right.$$
$$\div\left[S(1+S/100)(1+S/6.67)(1+S/1.67)\right.$$
$$\left.\left.\times\left(1+\frac{2*0.7}{20}S+\frac{S^2}{20^2}\right)\right]\right\} \quad (6)$$

Figure 4 shows the frequency response with the loop broken at the boresight error and with all significant frequencies marked. Since the phase is never less than -180 deg, the gain margin is infinite. Therefore, without additional phase lag in the loop, no amount of gain increase will make the closed-loop response unstable. For the parameters used, the phase margin is 53 deg. This phase margin improves with increasing stabilization loop gain and autopilot time constant as shown in Fig. 5. Since the open-loop transfer function is inversely proportional to seeker time constant, the stability will also improve with increasing seeker time constant as shown in Fig. 5. The seeker time constant cannot always be increased because of tracking requirements. Figure 5 shows that for a stabilization loop gain of 100 rad/s, the autopilot time constant required to yield 60 deg of phase margin (to leave room for sampling degradation) is 0.8 s. Doubling the seeker time constant increases the phase margin, which in turn allows the required autopilot time

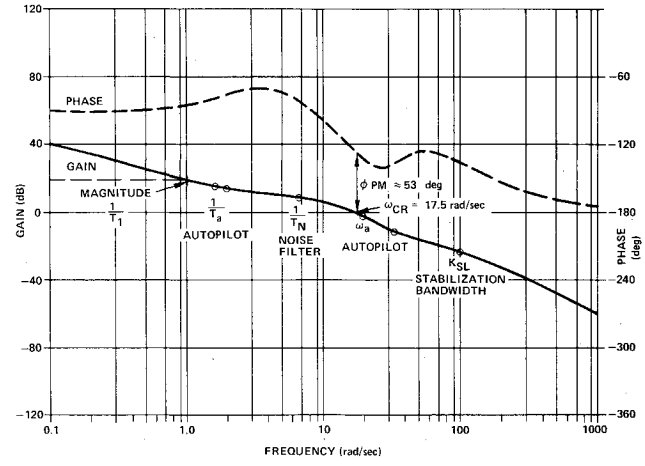

Fig. 4 Continuous frequency response for breaking loop at boresight error ($T_a = 0.6$ s).

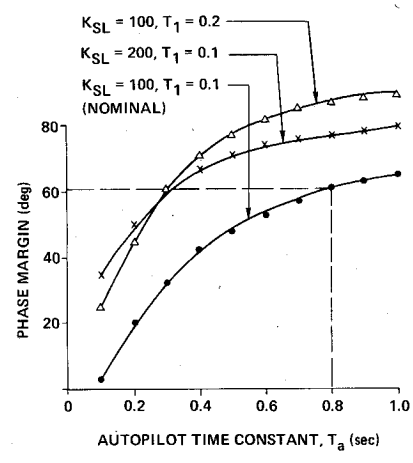

Fig. 5 Stability margins improve with increasing time constants and stabilization loop gain (loop broken at boresight error).

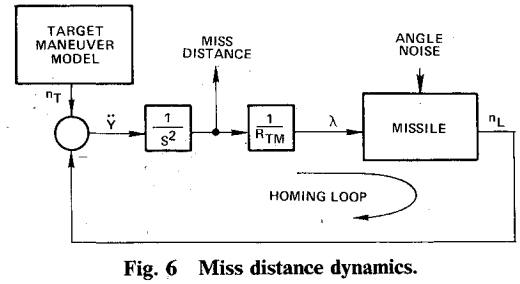

Fig. 6 Miss distance dynamics.

constant to be reduced to 0.3 s. In other words, with a seeker time constant of 0.1 s and an autopilot time constant of 0.8 s, the tracking loop phase could be decreased by 60 deg before the closed-loop response goes unstable. Similarly, with a seeker time constant of 0.2 s and an autopilot time constant of 0.3 s, the track loop phase could also be decreased by 60 deg before the closed-loop response goes unstable.

The relationship between miss distance and autopilot time constant was quantified utilizing the trajectory dynamic model of Fig. 6 in conjunction with an adjoint computer program that contained the parameters defined in Table 1 and error source values listed in Table 2. The adjoint results, plotted in Fig. 7, show the contribution of each component of miss to the total miss. As the autopilot time constant increases, the miss distance increases due to target maneuver and heading error, while it decreases due to glint noise. For the case considered, increasing the autopilot time constant increases the miss distance while improving the stability margins.

Table 2 Error sources

Error source	Value
Uniformly distributed target maneuver	1 g over 10 s
Heading error	10 deg
Glint noise	10 ft in 12.56 rad/s bandwidth
Range independent noise	1 mrad in 100 rad/s bandwidth
Receiver noise	20 mrad at 100 kft in 100 rad/s bandwidth

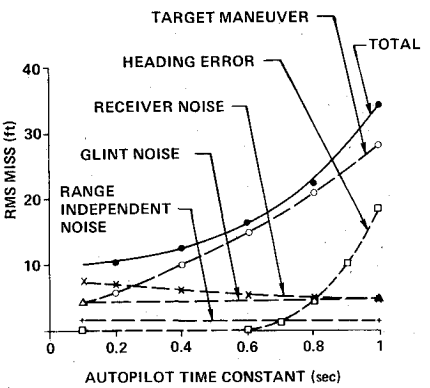

Fig. 7 Miss distance error budget for continuous system (nominal $-K_{SL} = 100$, $T_I = 0.1$).

Sampled Data Analysis

The systems under consideration are radar guided missiles. The sample and hold at the guidance command implies a system in which line-of-sight rate estimates from the noise filter in the missile are sampled, sent to the ground along with closing velocity information, processed (which in this case is simply the multiplication of the quantities $N'V_c\dot{\lambda}$), and sent back to the missile. The rest of the system is analog. The digital data rate should be low in order to maximize the number of missiles that a given ground complex can control. However, if the data rate is too low, guidance system instability can occur. A different type of system is implied by the sample and hold at the boresight error. In this system, boresight error is not available continuously. It is available only when the target is being illuminated by the ground radar. The data rate should be low in order to maximize the number of targets that a single radar can engage. Again, if the data rate is too low, the system becomes unstable. This paper explores the limits of these different digitally guided systems. It should be noted that only the guidance is digitized. Questions related to digitization of the autopilot or the seeker stabilization loop, which could lead to much higher data rates, are considered elsewhere.[9,10]

When the loop is broken at a sample and zero order hold, the continuous open-loop transfer function $HG(S)$ is modified by the Poisson summation.[11,12]

$$HG^*(S) = \frac{1}{T_s}\sum_{n=-\infty}^{\infty}\left[\left(\frac{1-e^{-sT_s}}{s}\right)HG(S)\right]_{s=s+jn\omega_s} \tag{7}$$

where the sampling time T_s obeys the relationship

$$\omega_s = \frac{2\pi}{T_s} \tag{8}$$

If the sampling time is small (ω_s large), most of the terms in the summation will be attenuated by the zero order hold and will be small compared to the primary term. In this case, the open-loop sample data transfer function can be approximated by

$$HG^*(S) \simeq \frac{1}{T_s}\left(\frac{1-e^{-sT_s}}{s}\right)HG(S) \tag{9}$$

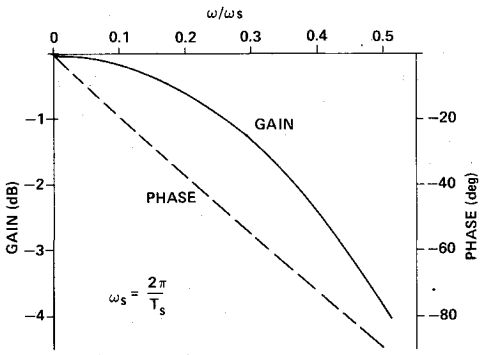

Fig. 8 Frequency characteristics of a sampler and zero order hold.

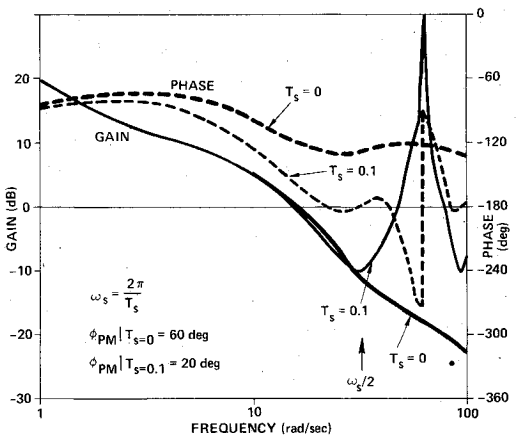

Fig. 9 Sampling increases phase lag, thus degrading phase margin (loop open at boresight error).

Therefore, the approximate transfer function of a sampler and zero order hold is[10]

$$\text{Sample and Hold} \simeq \frac{1-e^{-sT_s}}{sT_s} = \frac{\sin\dfrac{\omega T_s}{2}}{\dfrac{\omega T_s}{2}}\Big/\!\!\underline{\ -\omega T_s/2} \tag{10}$$

The gain and phase characteristics of this approximation to a sampler and zero order hold vs normalized frequency are displayed in Fig. 8. Here we can see that the sampler and zero order hold has approximately 0 dB of gain and phase lag linearly increasing with sampling time. This means that the introduction of a sampler and zero order hold into a loop can cause significant phase lag depending upon the sampling frequency ω_s. The stability margins will be adversely affected if the phase lag is significant in the vicinity of the crossover frequency of the loop transmission. Illustrations of the differences between continuous and sampled data open-loop transfer functions appear in Figs. 9 and 10. These Bode plots represent the attitude loop being broken at the boresight error (switches S1 up and S2 down in Fig. 1) and acceleration command (switches S1 down and S2 up in Fig. 1). Twenty-five terms were used in evaluating the Poisson summation required for the calculation of the sample data open-loop transfer function. Figure 9 shows the gains of both functions to be indistinguishable to a frequency of 30 rad/s, while the phase loss at this frequency is nearly 60 deg. For this case, the phase margin was reduced from 60 deg in the continuous case ($T_s = 0$ s) to 20 deg in the sampled data case ($T_s = 0.1$ s). Figure 10 also shows the gains of both functions to be quite similar to approximately 20 rad/s. However, the phase lag due to sampling causes the phase to cross 180 deg sooner (26 rad/s to 18 rad/s), resulting in a loss of nearly 5 dB in gain margin. Thus this type of digital homing system has degraded stability margins for most practical sampling times.

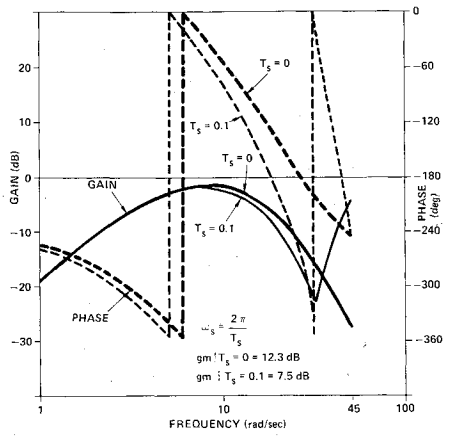

Fig. 10 Sampling increases phase lag, thus degrading gain margin (loop open at acceleration command, $T_a = 0.6$ s).

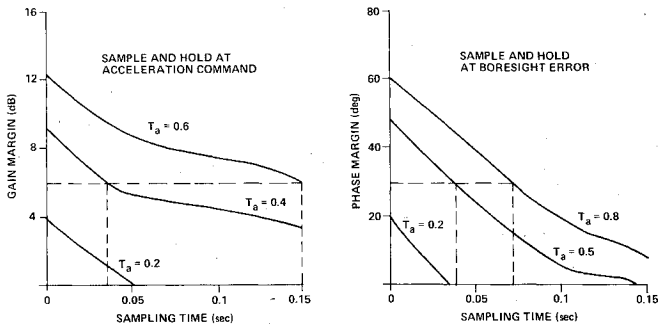

Fig. 11 Stability margin tradeoffs as a function of sample and hold location.

Sample data stability margins can be improved by either decreasing the sampling time or increasing the autopilot time constant. In addition, the sampler and zero order hold location is important in determining stability margins. Figure 11 shows some stability margin tradeoffs as a function of sample and hold location. If the acceleration command is sampled and held (switches S1 down and S2 up in Fig. 1) with a 6 dB gain margin requirement, Fig. 11 indicates that a 0.15-s sampling time is required to support an autopilot time constant of 0.6 s, while a 0.035-s sampling time is required to support an autopilot time constant of 0.4 s. A 0.2-s autopilot time constant cannot support sampling in this example. If the boresight error is sampled and held (switches S1 up and S2 down in Fig. 1) with a 30 deg phase margin requirement, Fig. 11 indicates that a 0.07-s sampling time is required to support an autopilot time constant of 0.8 s, while a 0.04-s sampling time is required to support an autopilot time constant of 0.5 s. Again, a 0.2-s autopilot cannot support sampling. This figure also shows that system requirements are considerably more stringent if the sampling is at the boresight error, rather than at the acceleration command.

Increasing the autopilot time constant improves the stability margins, but also degrades system performance in terms of increased miss distance due to target maneuver. Methods for maintaining performance and stability margins include increasing the stabilization loop gain and/or the seeker time constant. Of course, increasing the stabilization loop gain may not be possible because of increased cost, and increasing the seeker time constant may not be feasible because of seeker tracking dynamics and radar noise considerations.

If feasible, increasing the stabilization loop gain or increasing the seeker time constant are shown to be effective ways of improving the stability margins in Figs. 3 and 5. Figure 3 shows that doubling the stabilization loop gain (loop broken at acceleration command) allows a reduction in the autopilot time constant from 0.6 to 0.2 s for a 12-dB gain margin

Table 3 Minimum allowable autopilot time constants for constant stability margins

Condition	Minimum T_a: 12 DB gain margin loop broken at acceleration command, s	Minimum T_a: 60 deg phase margin loop broken at boresight error, s
$K_{SL} = 100$, $T_l = 0.1$	0.6	
$K_{SL} = 200$, $T_l = 0.1$	0.2	
$K_{SL} = 100$, $T_l = 0.1$		0.8
$K_{SL} = 100$, $T_l = 0.2$		0.3

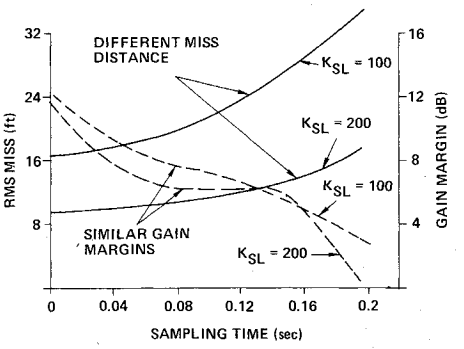

Fig. 12 Miss distance can be improved by increasing stabilization loop gain (sample and hold at acceleration command).

(continuous case). This means that with a stabilization loop gain of 100 rad/s and an autopilot time constant of 0.6 s, or with a stabilization loop gain of 200 rad/s and an autopilot time constant of 0.2 s, the autopilot gain can be increased by a factor of 4 (12 dB) before the closed-loop response goes unstable. Similarly, Fig. 5 shows that doubling the seeker time constant (loop broken at boresight error) allows a reduction in the autopilot time constant from 0.8 to 0.3 s for a 60 deg phase margin (continuous case). In other words, with a seeker time constant of 0.1 s and an autopilot time constant of 0.8 s, or with a seeker time constant of 0.2 s and an autopilot time constant of 0.3 s, the track loop phase lag can be increased by 60 deg before the onset of instability. These results, summarized in Table 3, indicate that such adjustments will improve system performance because the autopilot time constant can be reduced.

If the acceleration command is sampled (switches S1 down and S2 up in Fig. 1), stability-performance tradeoffs are presented in Fig. 12 for doubling the stabilization loop gain. For a requirement of 6 dB in gain margin, the miss distance can be reduced from 26.5 to 14 ft by doubling the gain. The increased gain allows the autopilot time constant to be reduced from 0.6 to 0.2 s, thus significantly reducing the target maneuver induced miss distance. If the boresight error is sampled (switches S1 down and S2 up in Fig. 1), stability-performance tradeoffs are shown in Fig. 13 for doubling the seeker time constant. The miss distance can be reduced from 23.5 to 17 ft by doubling the time constant for a phase margin requirement of 30 deg. The increase in seeker time constant allows the autopilot time constant to be reduced from 0.8 to 0.3 s, thus reducing the target maneuver induced miss distance.

Another method of improving the stability margins without increasing gains or decreasing the autopilot time constant is to introduce a lead-lag network after the sample and hold to shape the loop frequency response. The dynamics of this shaping are described by

$$\text{COMP} = \frac{1 + S/\omega_2}{1 + S/\omega_1} \tag{11}$$

where ω_1 is greater than ω_2. This shaping technique permits

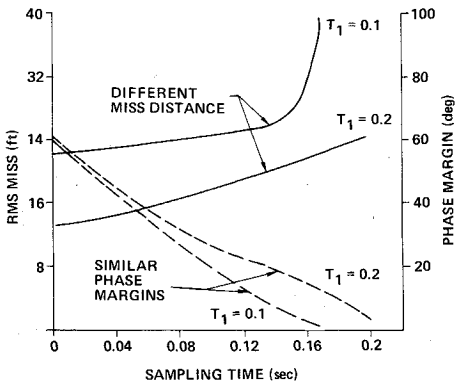

Fig. 13 Miss distance can be improved by increasing seeker time constant (sample and hold at boresight error).

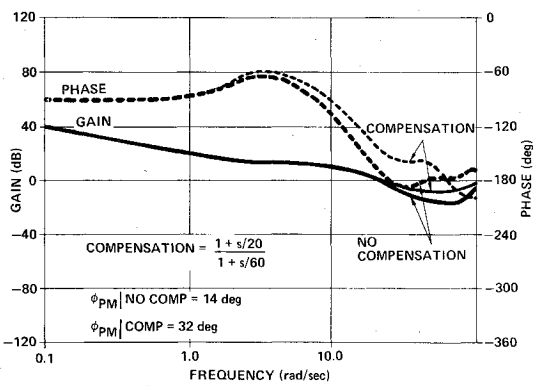

Fig. 14 Lead-lag compensation improves stability margin (loop broken at boresight error, $T_s = 0.05$ s, $T_a = 0.4$ s).

additional phase to be added to the system, thus compensating for the phase loss due to digitization. The larger the frequency difference between the lead and lag, the larger will be the phase contribution of the network. However, the frequency difference cannot be made overly large because of the high-frequency gain contribution of the network.

To illustrate the benefit of frequency shaping, a case was chosen in which the digitization occurred at the boresight error with a sampling time of 0.05 s. The open-loop Bode response for this system and an autopilot time constant of 0.4 s is shown in Fig. 14. With no digitization this system would have a phase margin of 42 deg (see Fig. 5). The digitization causes a significant loss of phase, resulting in a phase margin of only 14 deg as shown in Fig. 14. The phase margin for the digitized system could be increased by increasing the autopilot time constant to 0.6 s, resulting in a phase margin of 30 deg, or by introduction of the lead-lag network.

$$\text{COMP} = \frac{1 + S/20}{1 + S/60} \tag{12}$$

This network increases the phase margin from 14 to 32 deg, as can be seen from Fig. 14. Introducing the lead term at approximately the crossover frequency ensures that the new crossover frequency will be increased only slightly. The three to one separation between lag and lead frequencies provides significant phase contribution at the crossover frequency, thus dramatically improving the phase margin.

The introduction of the lead-lag compensation network improves the stability margins, thus allowing for a reduction in autopilot time constant that in turn improves the miss distance performance. For this example in which sampling was occurring at a rate of 20 Hz ($T_s = 0.05$ s) an autopilot time constant of 0.6 s was required to yield 30 deg of phase margin. The introduction of the compensation network allowed the autopilot time constant to be reduced to 0.4 s while keeping the phase margin at 32 deg. Thus miss distance performance, shown in Table 4, is better for the system having compensation and faster autopilot time constant because it's reduced the miss due to target maneuver. If the target accelerates at a higher level, the performance benefits derived from frequency shaped compensation are more substantial.

Conclusions

This paper considers digitization at two points in the homing guidance loop. The first point of digitization is at the acceleration command. This point has infinite phase margin and a finite gain margin which depends upon the autopilot time constant, the seeker tracking time constant, the stabilization loop gain, and the time between samples. Tradeoff curves show that gain margin degrades as autopilot time constant, tracking time constant, and stabilization gain reduce, and time between samples increases. The second point of digitization is at the seeker boresight error. This point has infinite gain margin and a finite phase margin which depends upon the autopilot time constant, the seeker tracking time constant, the stabilization loop gain, and the time between samples. Tradeoff curves show that phase margin degrades as autopilot time constant, tracking time constant, and stabilization gain reduce, and as time between samples increases. The goal is to choose the longest time between samples that the margins will allow in order to maximize the number of homing missiles the system can control or the number of targets that the system can engage.

For both systems, the miss distances resulting from all the parameter choices are shown as a benchmark to indicate that miss distance increases as stability margin degrades. It is clear from this data that each of the system design parameters is dependent upon the values of all of the other parameters. Therefore, all parameters must be examined if the preliminary design is to be balanced, constructible, and robust.

References

[1]Nesline, F.W., Jr. and Zarchan, P., "Missile Guidance Design Trade-Offs for High Altitude Air Defense," *Journal of Guidance, Control, and Dynamics*, Vol. 6, May-June 1983, pp. 207-212.

[2]Garnell, P. and East, D.J., *Guided Weapon Control Systems*, Pergamon Press, Oxford, 1977.

[3]Travers, P., "Interceptor Dynamics," unpublished lecture notes, Raytheon Co., Bedford, Mass., circa 1971.

[4]Zarchan, P., "Complete Statistical Analysis of Nonlinear Missile

Table 4 Miss distance error budget for compensated and uncompensated systems ($T_s = 0.5$ s, sampling at boresight error)

Error source	Value	No compensation $T_a = 0.6$ s, $\phi_{PM} = 30$ deg	Compensation $T_a = 0.4$ s, $\phi_{PM} = 32$ deg
Random target maneuver	1 g uniformly distributed over 10 s	15.1	10.1
Heading error	10 deg	0.01	0.2
Glint noise	10 ft in 12.56 rad/s bandwidth	5.5	6.1
Range independent noise	1 mrad in 100 rad/s bandwidth	2.4	2.6
Receiver noise	20 mrad at 100 kft in 100 rad/s bandwidth	7.2	6.9
rms		17.8 ft	14.0 ft

Guidance Systems-SLAM," *Journal of Guidance and Control*, Vol. 2, Jan.-Feb. 1979, pp. 71-78.

[5]Nesline, F.W. and Zarchan, P., "A New Look at Classical vs Modern Homing Missile Guidance," *Journal of Guidance and Control*, Vol. 4, Jan.-Feb. 1981, pp. 78-85.

[6]Nesline, F.W., "Missile Guidance for Low Altitude Air Defense," *Journal of Guidance and Control*, Vol. 2, July-Aug. 1979, pp. 283-289.

[7]Nyquist, H., "Regeneration Theory," *Bell System Technical Journal*, Vol. II, 1932, pp. 126-247.

[8]Bode, H.W., *Network Analysis and Feedback Amplifier Design*, D. Van Nostrand Company, Inc., Toronto, 1945, pp. 188-191.

[9]Nesline, F.W. and Nabbefeld, N.C., "Design of Digital Autopilots for Homing Missiles," *AGARD Conference Proceedings No. CP270*, Paper No. 29, 1979.

[10]Nesline, F.W. and Zarchan, P., "Hardware/Software Trade-Offs for Digital Flight Control of Guided Missiles," *AGARD 33rd GCP Symposium*, Oct. 13-15, 1981.

[11]Slater, L.I. and Levy, S.M., "Sample-Data Control Systems Analysis Using the Poisson Summation Rule," *IEEE Transactions on Aerospace and Electronic Systems*, Sept. 1974, pp. 630-635.

[12]Ragazzini, J.R. and Franklin, G.F., *Sample-Data Control Systems*, McGraw-Hill Book Company, New York, 1958.